Iraqi Journal of Physics, 2019 *Vol.17, No.43, PP. 49-57*

DOI: 10.20723/ijp.17.43.49-57

Gas Sensing of $(SnO_2)_{1-x}(ZnO)_x$ composite films associating with structural and electrical properties

Dunia Y. Khuder[1], Ramiz A. AL-Ansari[1], Hind F. Oleiwi[1], Ghuson H. Mohammed[2], Sarah A. Salman[3]

[1]Department of Physics, College of Science for Women, University of Baghdad

[2]Department of Physics, College of Science, University of Baghdad, Baghdad, Iraq

[3]Ministry of Education

E-mail: dunia9285@gmail.com

Abstract

Semiconductor-based gas sensors were prepared, using n-type tin oxide (SnO_2) and tin oxide: zinc oxide composite [$(SnO_2)_{1-x}(ZnO)_x$] at different atomic ratios (x) using pulsed laser deposition at room temperature, without any treatment. The prepared thin films were examined in order to obtain the optimum conditions for gas sensing applications, using X-ray diffraction, Hall effect measurements, and direct current conductivity. It was found that the optimum crystallinity and maximum electron density, corresponding to the minimum charge carrier mobility, appeared at 10% ZnO ratio. This sample has the optimum gas sensitivity was 358 % against 10% NO_2 gas appeared at 473 K working temperature.

Key words

Tin oxide, Zinc oxide, gas sensor, structural properties, electrical properties.

Article info.

Received: Jul. 2019
Accepted: Oct. 2019
Published: Dec. 2019

التحسس الغازي لأغشية مركب $(SnO_2)_{1-x}(ZnO)_x$ مع الخصائص التركيبية والكهربائية

دنيا ياس خضير[1]، رامز احمد محمد الانصاري[1]، هند فاضل عليوي[1]، غصون حميد محمد[2]، سارة عامر سلمان[3]

[1]قسم الفيزياء، كلية العلوم للبنات، جامعة بغداد

[2]قسم الفيزياء، كلية العلوم، جامعة بغداد، بغداد، العراق

[3]وزارة التربية

الخلاصة

تم تحضير المتحسس الغازي المعتمد على شبه الموصل، باستخدام أوكسيد القصدير(SnO_2) من النوع n و مزيج أوكسيد القصدير: أوكسيد الزنك $(SnO_2)_{1-x}(ZnO)_x$ عند نسب ذرية x مختلف باستخدام الترسيب بالليزر النبضي في درجة حرارة الغرفة، بدون اي معالجة. فحصت الأغشية الرقيقة المحضرة للوصول الى الظروف المثلى لتطبيقات المتحسس الغازي، باستخدام حيود الأشعة السينية، وقياسات تأثير هول، وتوصيلية التيار الكهربائي المباشر. وقد وجد أن درجة التبلور المثلى وكثافة الإلكترون القصوى، المقابلة لتحركية حاملات الشحنة الدنيا، تظهر عند النسبة 10% من ZnO. وكانت أعلى حساسية لغاز لثاني أوكسيد النيتروجين هي 358% عند تركيز 10% وعند درجة حرارة تشغيل 473 كلفن.

Introduction

Semiconductor-based gas sensors are important devices to monitor levels of pollution with hazardous gases (toxic and greenhouse gases) because of their low cost, high sensitivity and low response time [1].

Among the metal oxides semiconductors that extensively studied in the gas sensing, SnO_2 is

frequently used for many gasses sensing due to its numerous advantages such as simple manufacturing technique, low cost, and rapid response to a broad range of gases, but generally it requires a high working temperature beyond 573 K [2].

Since SnO_2 was demonstrated as a gas-sensing device in 1962 [3]. The SnO_2 sensors have been developed by many ways such as synthesize its nanocrystalline structures [4, 5], by combining different catalysts doped [6], and making a composite with other materials for the goal of high sensitivity and high selectivity for harmful gasses. SnO_2-ZnO sensors are more sensitive than the individual components tin dioxide or zinc oxide when tested in the same conditions. The most sensitive mixed sensor indicates an interactive effect between the two components [7].

There are several factors that affect the efficiency of the sensor, such as the nanoscale structure, the surface area of the active material and the degree of granularity connections, which depends on the preparation conditions [8]. The other influencing factors are the electrical characteristics, which include concentrations of the charge carriers and their mobility [9].

SnO_2 thin film was prepared by different techniques. Formation of nanocrystalline porous SnO_2 thin film can prepare utilize pulsed laser deposition technique for gas sensing applications [10].

The aim of this work is study the effect $(SnO_2)_{1-x}(ZnO)_x$ composite atomic ratio on its structural and electrical properties, then finally find the optimum $(SnO_2)_{1-x}(ZnO)_x$ composite thin film ratio for fabricating NO_2 gas sensor.

Experiment part

SnO_2 powder with 99.9% purity and ZnO powder with 99.9% purity were used. The targets were formed as cylindrical capsules of 1.5 cm diameter, by mixing the two powders by different atomic percentage and then pressed into a mold. Thin films were prepared using pulsed laser deposition technique under pressure of 10^{-2} mbar at without any treatment. ND-YAG pulse laser was used, with 1064 nm wavelength, pulse energy of 1000 mJ and pulse duration of 10 ns. The laser beam was focused on the targets using a lens with a focal distance of 10 cm through the glass chamber. The substrate is parallel to the target with 2 cm separation. The prepared thin films were examined without any treatment. The prepared films thicknesses were measured by using an optical spectroscopic reflectometer (TFProbe TM from Angstrom Sun Technology Inc.) which is about 170 nm for all films. The prepared samples were examined by X-ray diffraction (XRD) was measured using (SHIMADZU XRD600).

The electrical properties of $(SnO_2)_{1-x}(ZnO)_x$ thin films for different x atomic ratios were investigated by studying the variation of dc electrical conductivity with temperature and Hall effect measurements after appropriate aluminum electrodes deposition. The study of electrical conductivity as a function of the temperature determined activation energies. Thin films resistance was recorded for every 10 temperature degrees from room temperature to 573 K.

Hall Effect measurement was done by HMS-3000 VER3.52 system. It was used in order to determine the type of majority carriers, charge carrier concentration (n) and its mobility (μ) at room temperature for the prepared thin films. Hall coefficient (R_H) was calculated using the change in induced Hall voltages (V_H) with respect to current (I_H) in the presence of a

magnetic field perpendicular to the sample, throw which n and μ were calculated.
Finally, the prepared composite film at different ZnO atomic ratios were examined their sensitivity against 5% NO_2 gas.

Results and discussion

Fig.1 shows the X-ray diffraction (XRD) patterns for $(SnO_2)_{1-x}(ZnO)_x$ composite thin films at different ZnO atomic ratio. The XRD patterns demonstrate polycrystalline structure, for all prepared samples, matched with tetragonal SnO_2 standard card number 96-500-0225. Additional peaks appeared at the 15 and 20 % sample corresponding to ZnO crystals coordinated with the standard card No. 96-901-1663.

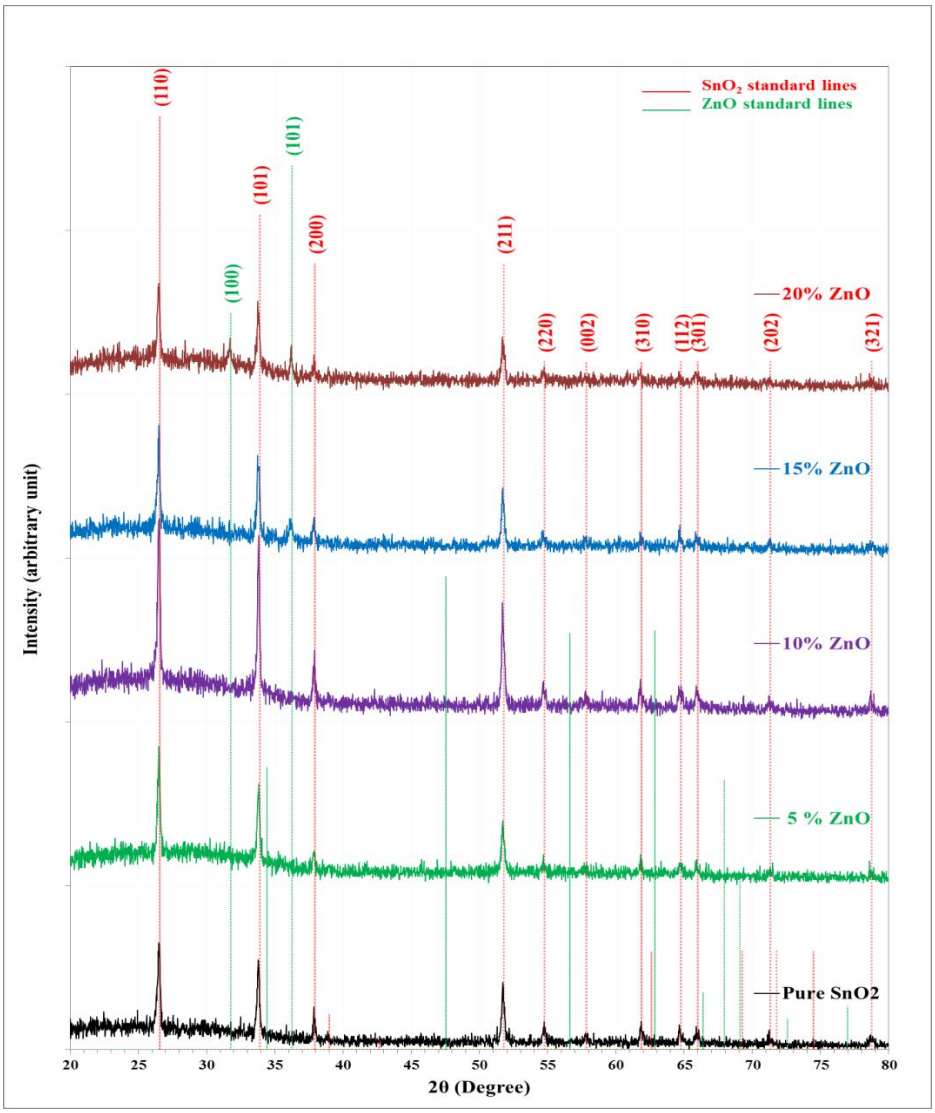

Fig.1: X-ray diffraction curves of pure SnO_2 thin film with different ZnO atomic ratios.

The interatomic distance (d_{hkl}) calculated by Bragg's law [11]

$$n\lambda = 2\, d_{hkl} \sin(\theta) \qquad (1)$$

where λ, θ and n represent X-ray wavelength from Cu target (1.5406 Å), diffraction angle and diffraction order respectively, while the crystalline size (C.S) was calculated using Scherrer equation according to full width at half maximum (FWHM) of the preferred peaks [12].

$$C.S = \frac{0.9\,\lambda}{FWHM\,.cos(\theta)} \qquad (2)$$

Table 1 shows the Bragg angle (2θ) of preferred orientation peak along (110) for SnO_2 structure, their intensity, d_{hkl}, C.S at different ZnO atomic ratio. The maximum intensity appeared at 10% ZnO. The maximum value for C.S is 34.5nm appeared at 10% ZnO atomic ratio. There is a small shift in peak location due to strain in lattice and lattice defect.

Table 1: 2θ, their intensity, experimental and standard d_{hkl}, FWHM and C.S for (110) peak of SnO_2 at different ZnO atomic ratio.

Sample	2θ (Deg.)	Int. (arb. unit)	d_{hkl} Exp.(Å)	d_{hkl} Standard(Å)	FWHM (Deg.)	C.S (nm)
Pure SnO_2	26.5248	114.9	3.3577	3.3496	0.3309	24.7
5% ZnO	26.5248	142.9	3.3577	3.3496	0.3309	24.7
10% ZnO	26.5721	212.3	3.3519	3.3496	0.2364	34.5
15% ZnO	26.6194	136.7	3.3460	3.3496	0.2837	28.8
20% ZnO	26.5248	103.5	3.3577	3.3496	0.2364	34.5

Fig.2 shows the change in logarithm of electrical conductivity Ln(σ) of the $(SnO_2)_{1-x}$ $(ZnO)_x$ thin films with the reciprocal temperature. In general, the electrical conductivity of semiconducting materials is increased by increasing temperature due to the increment of free charge carrier's concentration [13]. All samples have two conduction mechanisms, at two temperature ranges. The activation energies within the range (298-353 K) (E_{a1}) depend on the impurities where the conductivity is due to the transfer between the localized states levels within the energy band gap. While, the activation energy within the range (353-443K) (E_{a2}) depends on the transition between the extended levels of the valence and conduction bands [14].

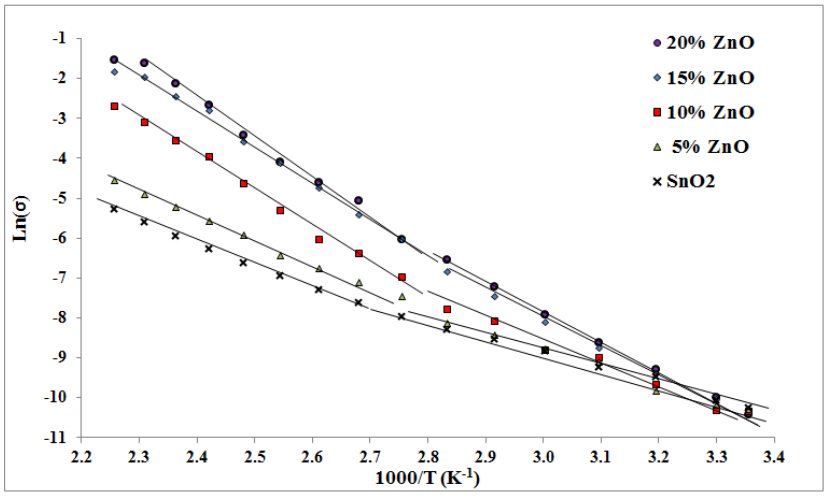

Fig. 2: Electrical conductivity logarithm with reciprocal temperature for $(SnO_2)_{1-x}$ $(ZnO)_x$.

Table 2 shows the DC activation energies at room temperature and their temperature ranges. The results showed that the activation energies in general increased with increasing the ZnO atomic ratio, maybe due to variation in energy gap, as shown in Fig.3. The dc conductivity at room temperature slightly decreases from 3.44×10^{-5} to 2.98×10^{-5} $(\Omega.cm)^{-1}$ with increasing of ZnO atomic ratio in the sample to 20% due to reducing sample mobility [15] as illustrated in Table 1.

Table 2: Activation energies, thermal ranges and dc conductivity of $(SnO_2)_{1-x}$ $(ZnO)_x$ thin films.

ZnO atomic (%)	E_{a1} (eV)	Range (K)	E_{a2} (eV)	Range (K)	σ_{RT} ($\Omega^{-1}.cm^{-1}$)
0	0.341	298-353	0.454	353-443	3.44E-05
5	0.385	298-353	0.523	353-443	3.40E-05
10	0.419	298-353	0.792	353-443	3.24E-05
15	0.563	298-353	0.806	353-443	3.20E-05
20	0.618	298-353	0.797	353-443	2.98E-05

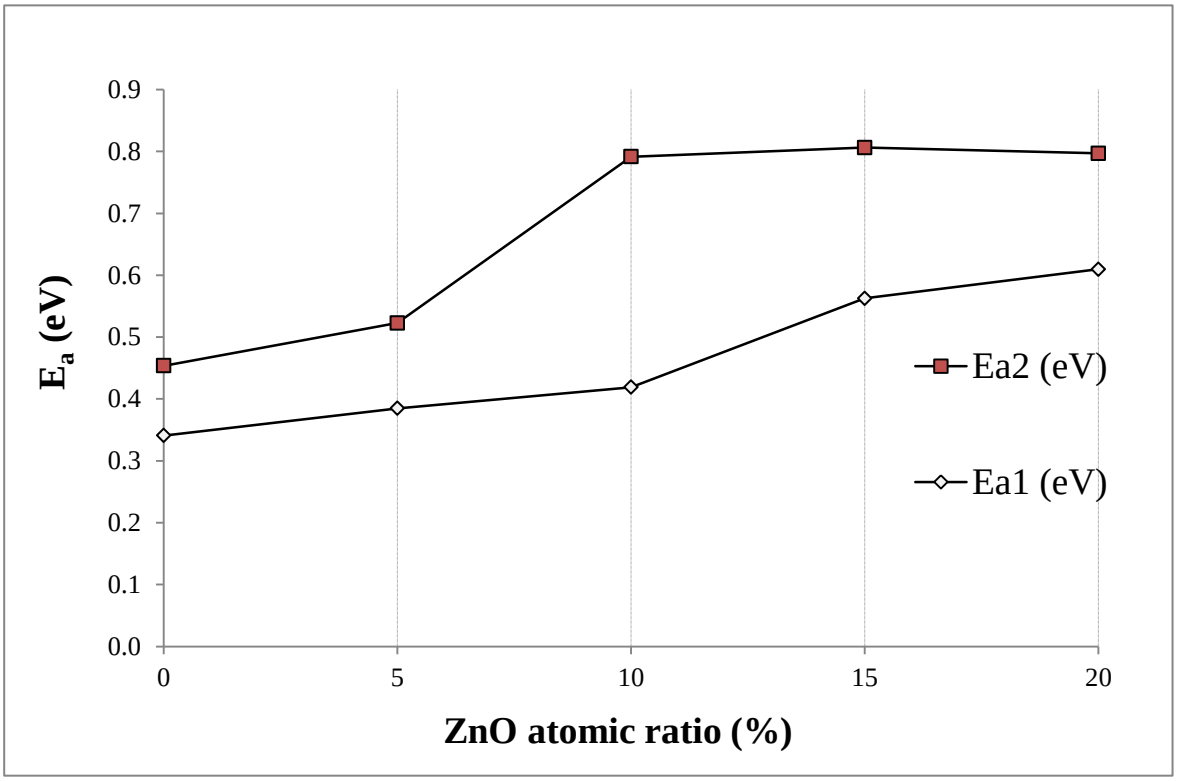

Fig.3: Variation of activation energies with ZnO atomic ratio in prepared samples.

Hall Effect measurement shows that all prepared samples were n-type. The material electrical conductivity depends on carrier's concentration and their mobility. Both mobility and carrier concentration are temperature and impurity dependent. The increase in ZnO to 10% cause an increase in the carriers concentration from 1.36×10^{12} to 1.288×10^{13} cm^{-3} and decreased at 20% ZnO atomic ratio to 2.08×10^{12} cm^{-3}, While the minimum mobility appeared at 10% ZnO atomic ratio, with opposite behavior of charge carrier concentration (as shown in Figs. 4 and 5). There are two basic types of scattering mechanisms that influence the mobility of charge carriers: lattice scattering and impurity scattering [16].

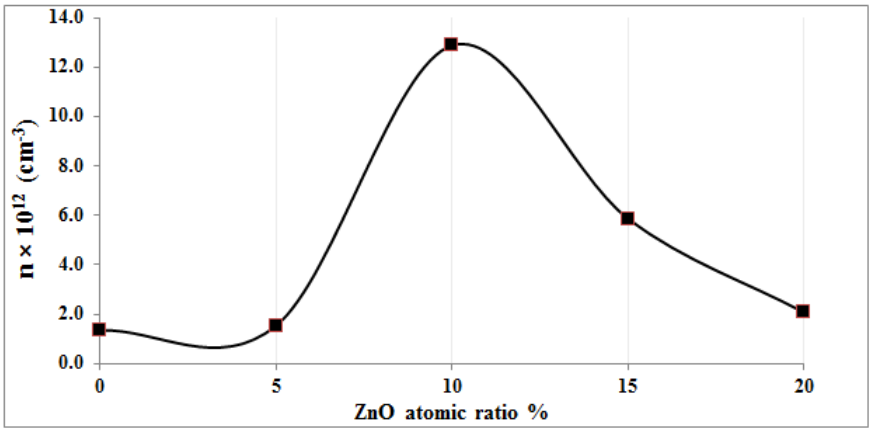

Fig.4: Variation in charge carrier density with ZnO atomic ratio.

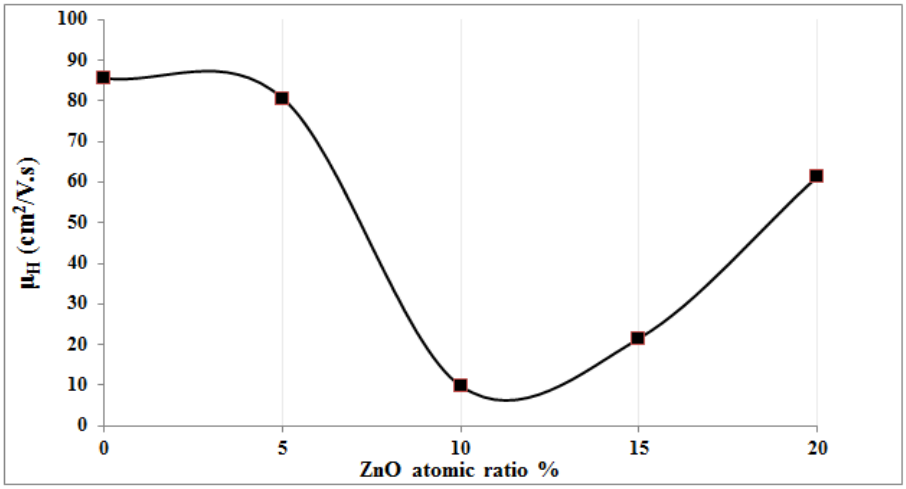

Fig. 5: Variation of mobility with ZnO atomic ratio.

Figs. 6 to 10 show the variation in the resistance with time at opening and closing of the NO_2 gas with 5% for the blend samples at different ZnO atomic ratios (0, 5, 10 15 and 20%) respectively. The sensing was examined at 473 and 573 K operating temperature, where the samples sensitivity was very weak at room temperature. Samples behaved as n-type semiconductor, where they increased their resistance when exposed to NO_2 gas, which is an oxidized gas.

The target gas interacts with the adsorbed oxygen ions on sample surface, which results in a change in charge carrier concentration. This change in charge carrier concentration serves to alter the resistivity of the material. Oxidizing gas causes to increase the depletion layer of charge carrying electrons from the sensing layer, resulting in a decrease in conductivity [17].

The sensing mechanism based on chemisorption of NO_2 according to the following reaction: $NO_{2\ (gas)} + e^- \rightarrow NO_2^-$ [9]. Electrons are extracted from the SnO_2 surface lead to increase the sample resistance. Then the NO_2^- ions are dissociated into $NO_{(gas)}$ and O^- as: $NO_2^- \rightarrow NO\ (g) + O^-$, where the generated O^- ions contribute to a further increase in the resistance [9]. It is appeared that all samples have sensitivity at 473 K higher than at 573 K working temperature due to the change in the efficiency of the interaction with different oxygen species [7].

The maximum sensitivity appeared at 10% ZnO ratio. The variation in gas sensitivity in different samples with different ZnO atomic ratios due to the variation in charge carriers density [7]. The maximum sensitivity associated with the maximum charge carrier concentrations.

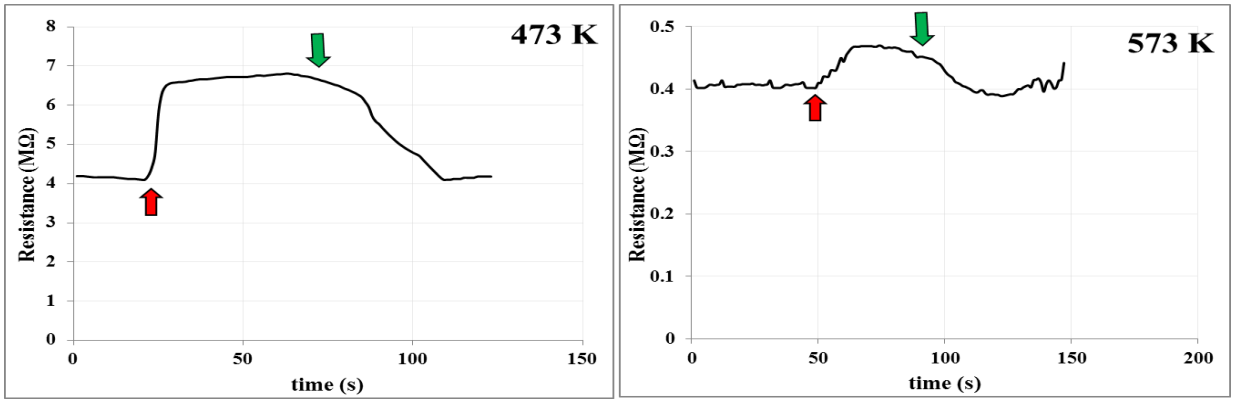

Fig.6: Variation of resistance of the SnO_2 sample when opening and closing of 5% NO_2 gas at 473 and 573 K.

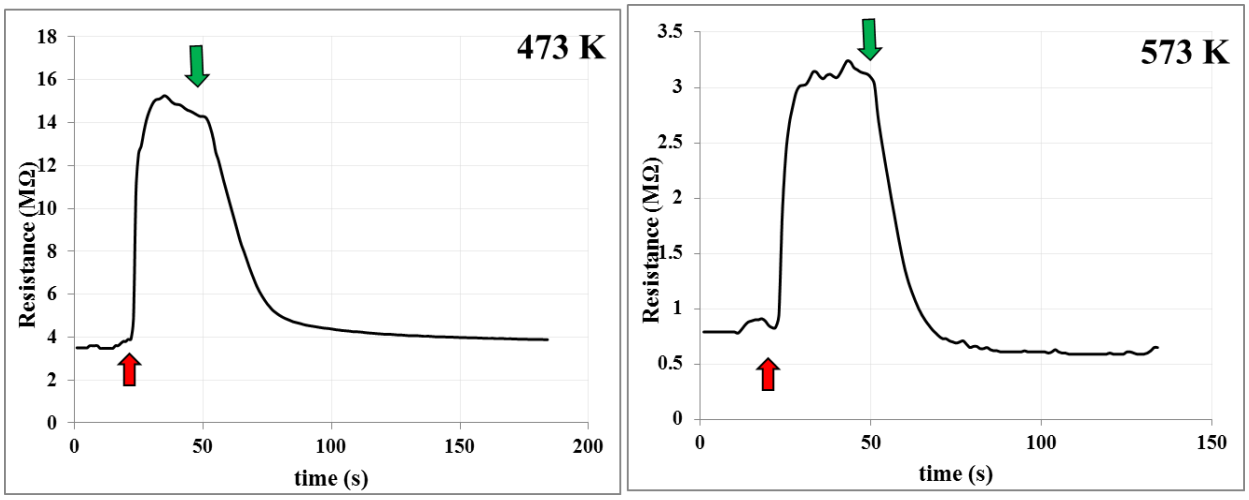

Fig. 7: Variation or resistance of the $(SnO)_{0.95}(ZnO)_{0.05}$ sample when opening and closing of 5% NO_2 gas at 473 and 573 K.

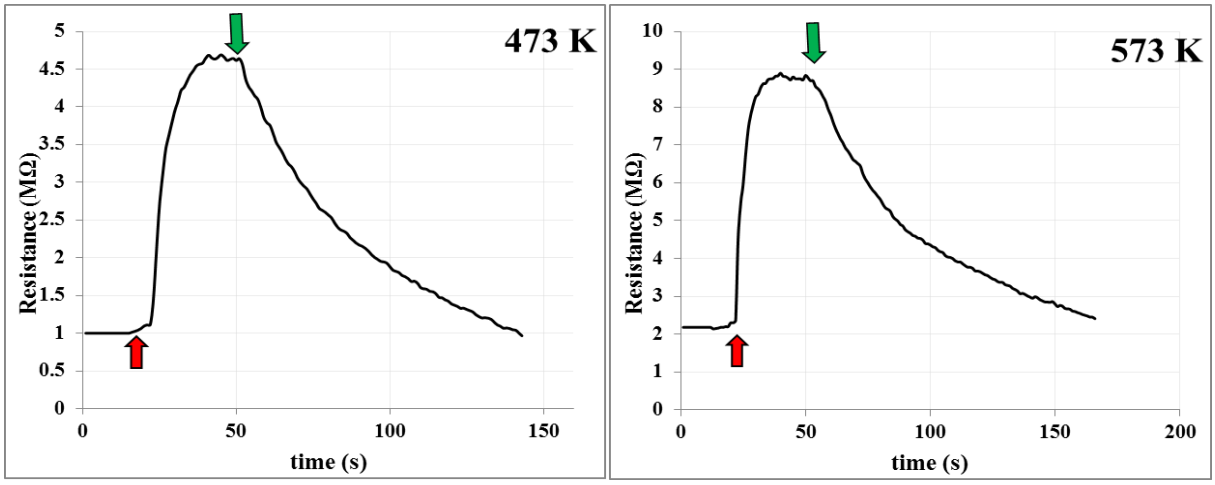

Fig. 8: Variation of with time for $(SnO)_{0.9}(ZnO)_{0.1}$ sample when opening and closing of 5% NO_2 gas at 473 and 573 K.

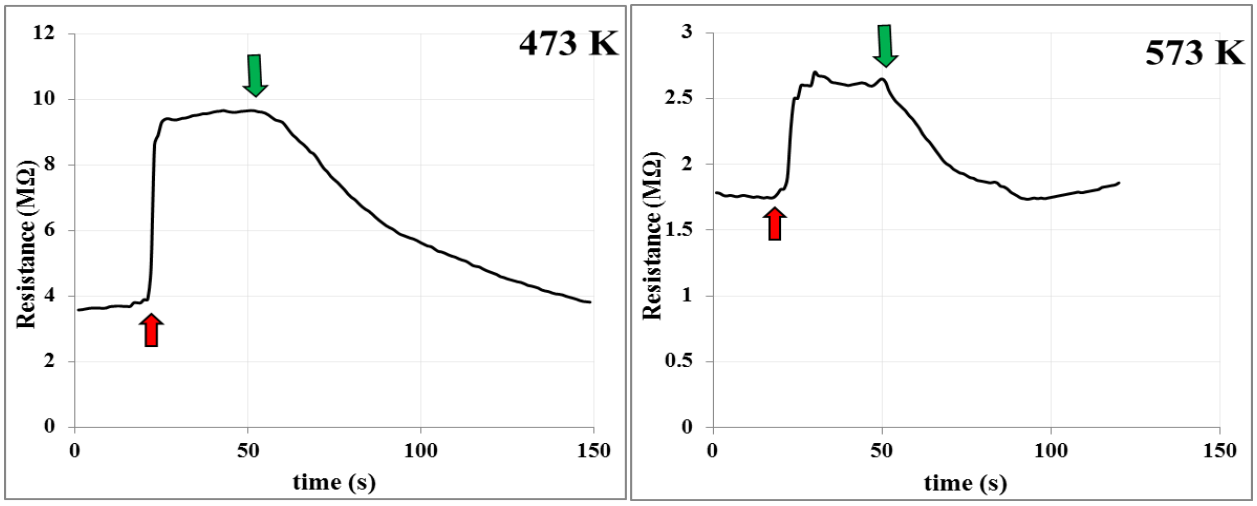

Fig. 9: Variation of with time for $(SnO)_{0.85}(ZnO)_{0.15}$ sample when opening and closing of 5% NO_2 gas at 473 and 573 K.

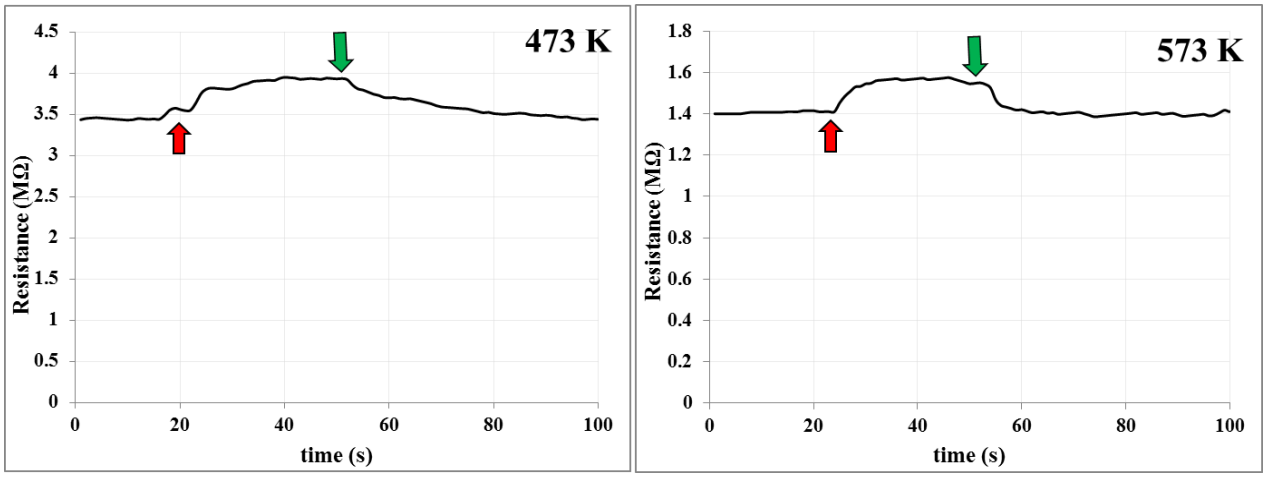

Fig.10: Variation of with time for $(SnO)_{0.8}(ZnO)_{0.2}$ sample when opening and closing of 5% NO_2 gas at 473 and 573 K.

Fig.11 shows the variation in the gas sensitivity with ZnO atomic ratios toward 5%NO_2 gas at 473 and 573 K.

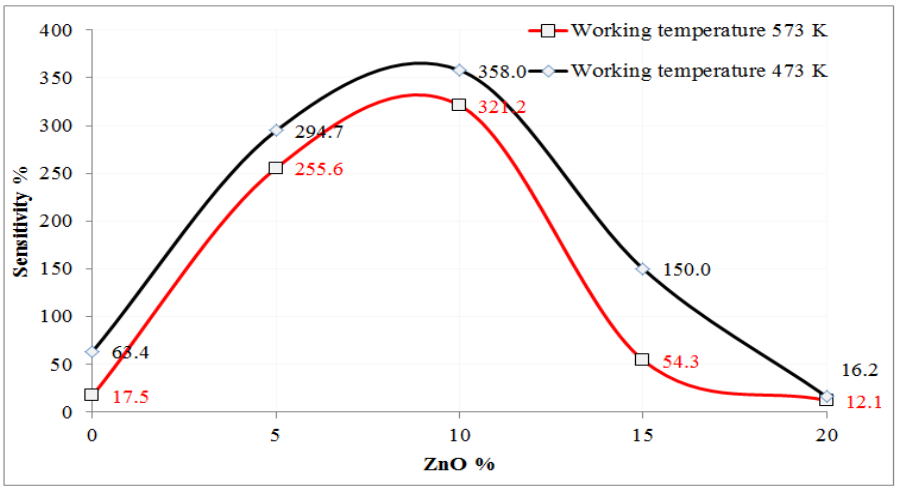

Fig.11: Variation of sensitivity with ZnO atomic ratio for $(SnO_2)_{1-x}(ZnO)_x$ thin films.

Conclusions

The results of examination of $(SnO)_{1-x}(ZnO)_x$, prepared by PLD technique, illustrate polycrystalline structures for all prepared samples. The maximum crystallinity at 10% ZnO ratio.

D.C activation energies increase with increasing ZnO atomic ratios. Maximum charge carrier concentration, corresponding to the minimum charge carrier mobility, appeared at 10% ZnO ratio. This ratio appeared has the optimum NO_2 gas sensitivity, which is equal to 358% at 473 K working temperature.

The gas sensitivity for all $(SnO)_{1-x}(ZnO)_x$ composite sample at different atomic ratios (x=0, 5, 10, 15 and 20%) against nitrogen oxide gas was very weak at room temperature, while it was clear at 473 K and decreased at 573 K.

References

[1] M. Cho, J. Yun, D. Kwon, K. Kim, I. Park, ACS Appl. Mater Interfaces, 10 (2018) 12870-12877.

[2] S. Bera, S. Kundu, H. Khan, S. Jana, J. Alloys Compd., 744 (2018) 260-270.

[3] B. Wei, M. Hsu, P. Su, H. Lin, R. Wu, H. Lai, Sensors Actuators, B Chem., 101 (2004) 81-89.

[4] O. Lupan, N. Wolff, V. Postica, T. Braniste, Ceram. Int., 44, 5 (2018) 4859-4867.

[5]Y. Li, N. Chen, D. Deng, X. Xing, X. Xiao, Y. Wang, Sensors Actuators, B Chem., 238 (2017) 264-273.

[6] Tianjiao Qi, J. Sun, X. Yang, F. Yan, J. Zuo, Sensors, 19, 14 (2019) 3131-1_3131-13.

[7] H. Ren, C. Gu, S. W. Joo, J. Cui, Y. Sun, J. Huang, Mater. Express, 8, 3 (2018) 263-271.

[8] Y. Sun, S. Liu, F. Meng, Sensors, 12, 3 (2012) 2610-2631.

[9] S. Kim, H. Na, H. Kim, V. Kulish, P. Wu, Sci. Rep., 5 (2015) 1-12.

[10] E. Preib, T. Rogge, A. Krauß, H. Seidel, Procedia Eng., 120 (2015) 88-91.

[11] W. H. Bragg and W. L. Bragg, X Rays and Crystal Structure. London: G. Bell and Sons, LTD., 1918.

[12] P. Scherrer, "Göttinger Nachrichten Gesell," Univ. zu Göttingen, vol. 2, p. 98, 1918.

[13] William D. Callister, Materials Science and Engineering An Introduction, 7th Editio. USA: John Wiley & Sons Inc., 2007.

[14] W. Tsang, E. Schubert, J. Cunningham, Appl. Phys. Lett., 60 (1992) 115-117.

[15] Q. Humayun, M. Kashif, U. Hashim, J. Nanomater., 2013 (2013) 1-8.

[16] S. Singh, P. Thiyagarajan, K. Kant, J. Phys. D Appl. Phys., 40 (2007) 6312-6327.

[17] G. Fine, L. Cavanagh, A. Afonja, R. Binions, Sensors, 10 (2010) 5469-5502.